Proceedings of ASME Turbo Expo 2011
GT2011
June 6-10, 2011, Vancouver, British Columbia, Canada

GT2011-46652

SWIRL-ENHANCED INTERNAL COOLING OF TURBINE AIRFOILS, PART 2 – 90 DEGREE FLOW ENTRY

Del Segura and Sumanta Acharya

Louisiana State University
Turbine Innovation and Energy Research (TIER) Center
Department of Mechanical Engineering
Baton Rouge, LA 70803, U.S.A.

ABSTRACT

Heat transfer measurements and analysis have been performed on a uniquely designed multi-channel passage consisting of a slot shaped channel with a 3:1 aspect ratio with coolant-feed tubes located adjacent to the main slot shaped channel. Small round jets connect the outer feed passages to the main channels at a 15 degree angle relative to the main channel flow direction and at a position tangent to the floor/roof of the main channel. Flow entering the multi-channel passages is directed into the main channel through orifices that reduce the pressure in the main channel, thereby enabling positive pressure differences between the feed and the main channel and allowing high velocity flow through the jets. The flow enters the main channel via a 90-degree turn through the orifice. The resulting flow through the side jets and main channel causes high shear flow along the roof and floor of the channel where the jet flow enters the main channel, swirl motion as the high velocity side jet flow enters the main channel flow at an angle relative to the main flow direction, and high turbulence regions as the lower velocity main channel flow tumbles when coming in contact with the high velocity jets issuing from the side channels.

The heat transfer characteristics were compared to the slot channel with a 90 degree inlet with no additional heat transfer enhancements. Four different jet configurations are presented along with three different orifice diameters. While a single channel passage with flow exiting freely is not a design typically found in a turbine airfoil, the benefits of this unique concept can be a basis for further studies with geometries more typical of a production airfoil.

The results yield average normalized Nusselt numbers enhancement for the entire main channel as high as 10.7, when compared to a smooth slot channel without heat transfer enhancements. Pressure losses, mainly due to the orifices, were high but the overall performance shows significant improvements when compared to other heat transfer enhancement methods in turbine airfoil mid-span regions.

INTRODUCTION

The quest to achieve greater efficiencies in turbine engines challenges turbine airfoil designers to seek new and innovative cooling strategies. The designs must be simple, inexpensive, and reliable. Current turbine inlet temperatures (~1500 ^{0}C) exceed the limits of airfoil material (~1000 ^{0}C) and must be cooled to avoid catastrophic failures. A portion of the compressor air is bypassed, redirected into passages in the turbine airfoil where this cooler air (~650 ^{0}C) reduces the external airfoil temperature to acceptable levels. As shown in figure 2, the common configurations for airfoil cooling include ribs, pin-fins, impingement jets, and film cooling holes [1]. Efficiency improvements can be realized when the amount of compressor bypass air, used for cooling the various components of the engine, is reduced.

The current mainstream internal cooling strategies add ribs to a smooth channel to induce vortices and flow reattachment as the fluid passes over the rib. The concept can be seen in Figure 1. The shape, angle, height, pitch, and layout of the ribs in the flow channel can affect the local and regional heat transfer in many ways. In figure 1, note how the turbulence intensity increases from very low intensity at the side walls to higher intensity near the center and along the flow path in this rib configuration.

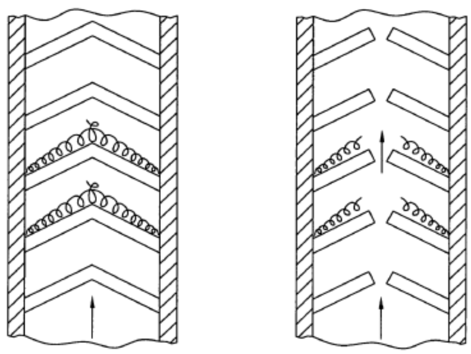

FIGURE 1: CONCEPT OF TURBULENCE INDUCED BY TRIP S TRIPS IN RECTANGULAR CHANNELS. [2].

Wang, et-al [3] performed a detailed study of various rib shapes in a square ducts with a rib pitch to rib height ratios varying from 8 to 15 and rib height to hydraulic diameter value of 0.1. The range of Reynolds numbers tested was 8,000 to 20,000. The highest Nu/Nu_o values occurred with the rib pitch to rib height ratio of 12 at Re=20k. Overall thermal performance (OTP) values were not presented. Taslim, et-al [4] tested several different rib configurations and determined a rib height to hydraulic diameter value of 0.125 provided the best results. They presented overall thermal performance (OTP) values as high as 1.9 at Re=10k to 1.5 at Re=25k. Many other studies show similar findings. The rib pitch and rib heights, as related to hydraulic diameters in these studies were used as guidelines in determining the jet diameters and jet pitch used in this study.

Kurtbaş, et-al [5] studied the effects of inducing swirl into a smooth channel by using flow directed swirl generator nozzles at the inlet of a round channel with uniform heat flux. Cone insert angles of 30^o, 45^o, and 60^o and flow director angles of 30^o, 60^o, and 90^o were examined. Reynolds numbers of 9,400 to 35,000 were used throughout the various test performed. Pressure drop was also measured and finally an overall thermal performance value was determined. The results yielded overall thermal performance (OTP) values ranging from 2.2 at Re=10k to 1.2 at Re=35k.

High heat transfer enhancement values were noted in studies utilizing swirl/cyclone motion in round internal passages with rectangular shaped side jets [6, 7]. Local thermal performance values (OTP) of 4-5 are reported, which yield substantial improvements when compared to similar passages with more conventional types of heat transfer enhancements. There have been a limited number of publications with other configurations utilizing swirl enhancements.

Swirling flows in channels provide the benefits of longer residence times, higher turbulence levels and can be combined with other heat transfer enhancements. A specific variant of this technique is the concept of lattice cooling [8] where a lattice network is used to increase the flow path, and combined with the associated impingement and trip-strips produced high heat transfer coefficients. Local values of Nu/Nu_o in the impingement areas are in the range of 6-10. The penalties paid for the improved cooling include, high pressure drops and the added weight of the lattice structure.

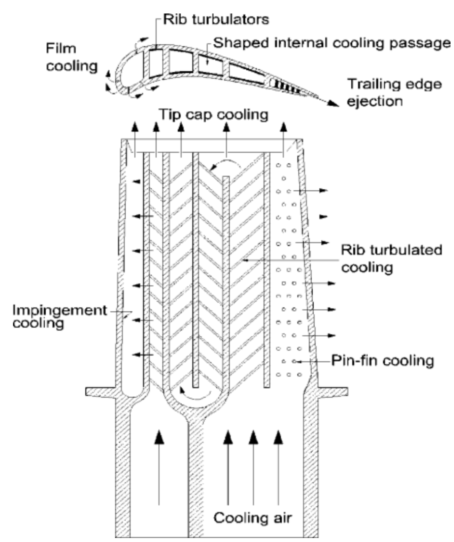

FIGURE 2: CROSS SECTION OF TYPICAL TURBINE BLADE WITH INTERNAL COOLING [1]

This study examines a novel configuration where the main coolant passage (a 3:1 AR passage) is fed by side slots that introduce high blowing ratio jets tangentially at discrete locations. These tangential jets induce a swirl motion in the slot shaped main channel cross flow air. The main channel cross flow air is introduced radially via a 90-degree turn through orifices tailored for the needed pressure drops. The orifices are the major contributors to the pressures losses and by changing the diameter of the orifices the effective blowing ratio can be controlled and adjusted to a specific application.

Several side-injection configurations are examined. The results are presented as normalized heat transfer enhancements, overall thermal performance, and pressure losses. The objective is to find a strategy that will produce high heat transfer enhancements that would offset the pressure drop penalty. Although the outer jet supply channels play in integral role in this design, the heat transfer enhancement is these channels are not considered in this study. In a real world practical application, the outer jet supply channels would have their own heat transfer enhancement strategy.

NOMENCLATURE

A	Cross section area, m^2
a	Width of slot channel, mm
b	Height of slot channel, mm
AR	Aspect Ratio, a/b
BR	Blowing Ratio
BFM	Back Flow Margin
C	Discharge coefficient
d	Jet hole diameter, mm
d_h	Channel Hydraulic Diameter, m
f	Friction Factor in the Channel
f_o	Friction Factor in a smooth round pipe
h	Convection Heat Transfer Coefficient, $W/m^2\,K$
k	Coefficient of thermal conductivity, $W/m\,K$
L	Channel Length, mm
M	Mach number
$\dot{m}$	Mass flow rate, (kg/s)
N_u	Nusselt Number
N_{uo}	Nusselt Number for a smooth round pipe
p	Pitch, mm
Pr	Prandtl Number
P	Pressure, Pa
P_m	Pressure, Main Channel, Pa
P_o	Pressure, Outer Jet Supply Channel, Pa
ΔP	Total Pressure Loss in Test Piece
R	Gas constant, $J\,K^{-1}\,mol^{-1}$
Re	Reynolds Number
t	time, s
T_w	Wall temperature, K
T_i	Initial temperature, K
$\Delta T_{m,i}$	Temperature difference between each time step, s
T_m	Fluid centerline temperature, K
U_m	Mean Velocity, m/s
Z	Compressibility factor

Greek

α	Coefficient of thermal diffusivity, m/s^2
ρ	Density, kg/m^3
τ	Time step for each temperature step, s

CONFIGURATIONS STUDIED

A 3:1 single passage slot shaped channel with a hydraulic diameter d_h of 0.0248m and a L/d_h of 8.7 is chosen for this study. The various configurations investigated to enhance heat transfer include several fluidic-swirl-generation configurations where the swirl is generated by introducing tangential jets along the side walls of the main coolant passage at a 15 degree angle relative to the main channel flow direction (Figure 3).

High pressure air is introduced into two round 15.9 mm diameter outer channels. Some of the air is directed through orifices; before entering the main 15.9 mm high by 47.7 mm wide slot shaped channel through a 90 degree entry angle. The air in the outer jet supply channels feed the 1.6 mm diameter jets. This results in a d/b ratio of 0.1, a typical effective ratio used for trip strip heat transfer enhancement [3, 4].

A typical fluidic swirl-generation configuration is shown in figure 3.

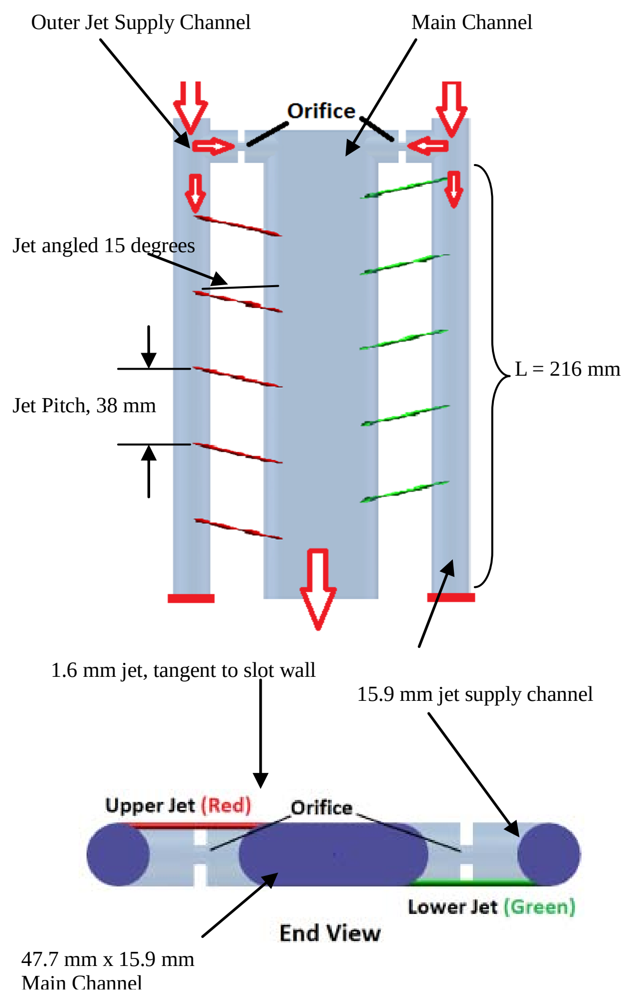

FIGURE 3: TOP & END VIEW OF TYPICAL FLUID PASSAGES.

The end view image shows the two round outer jet of 15.9 mm diameter feed channels with red upper jets and green lower jets supplying air to the main channel along a path that is tangent to the upper and lower walls of the main channel. The location of the two orifices, one on either end of the entry to the main channel, is also shown.

The orifices were removable and testing was performed with orifices of 3.18 mm, 3.94 mm, and 4.76 mm diameters. The ends of the outer jet supply channels are blocked. Therefore, all air entering the jet supply channels must exit through the jets.

The orifices are situated in a passage that connects the outer jet supply channels to the main channel as shown in figure 2. The orifices shape and manufacturing tolerances were in compliance with international standards established by ISO 5167 standards. Figure 4 shows the dimensions of one of the three orifice sets.

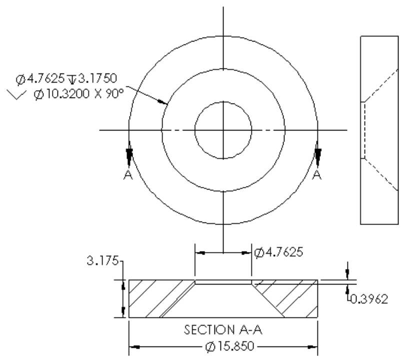

FIGURE 4: DETAILED VIEW OF 4.76 mm ORIFICE.

Four different jet configurations were tested, each with three different diameter orifices. The jet diameter remained the same for all tests at 1.6 mm.

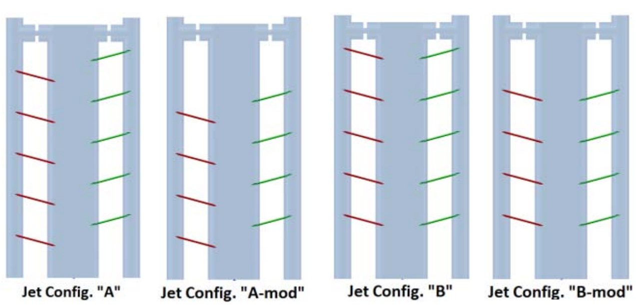

FIGURE 5: FOUR DIFFERENT FLUID PASSAGE CONFIGURATIONS

The four jet configurations tested are shown in figure 5. Jet configuration “A” uses five jets issuing from each jet supply channel. In this configuration, the jets are staggered across from one another by 19 mm. The resulting ratio of jet stagger (pitch) to jet diameter is 12. Again, this value has shown to be an effective pitch to trip strip height ratio when trip strip enhancements are used. Jet configuration “A-mod” is the same as configuration “A”, except the first series of jets are blocked. Configuration “B” also has five jets issuing from each side. The main difference between configuration “A” and “B” is that the jets are aligned across from one another. Configuration “B-mod” differs from configuration “B” by having the first series of jets blocked.

In addition to the four configurations listed above a series of baseline tests were performed with the orifices removed and all jets blocked. This configuration tests the heat transfer enhancement of a smooth slot shaped channel with a 90 degree entry. Main channel Reynolds numbers of 10k, 25k, 40k, and 50k were tested and this configuration was used to normalize all tests performed with jets and orifices.

A channel-average blowing ratio, jet velocity to main channel velocity, varied with each orifice diameter. The average blowing ratio was calculated based on the measured pressure drops in the main channel and the side channels, and is an average value across all the jet-holes. The individual jet-blowing ratio may vary from hole to hole depending on the pressure drop.

Large values of blowing ratios were needed to ensure that the jet penetrated the main flow field to the other side, and potentially create an impingement effect. The total mass flow rates combined with the hydraulic diameter of the main channel were used to define the Reynolds number of the flow. The results of all tests presented in this paper are compared (normalized) with the non-enhanced smooth channel designated by $Nu_{90\ smooth}$.

In most of the color contour plots shown in this paper, it was necessary to use different scales to accent notable heat transfer regions. In order to more easily differentiate various configurations line plots of the average values are also presented.

EXPERIMENTS

Experimental Apparatus

A simulated clear polycarbonate airfoil was built that incorporates two strategies for inducing swirl motion in the internal passages of an airfoil. The main cooling channel is slot shaped with and aspect ratio of 3:1, with a height of 15.9 mm and a width of 47.6 mm. The overall length of the slot channel is 216 mm, not including the 90 degree transition entry and radiused exit portion of the channel.

The side-jets that produce swirl are fed through outer passages that run parallel to the main slot shaped channel. These passages are 15.9 mm in diameter and the diameter of the jet at the entrance to the main channel is 1.6 mm. The flow into the jet supply channels was not through flow and could only exit through the jets. In configurations "A" and "B" the jets were spaced 38 mm apart along one side. In configuration "A", the jets located on the opposite wall were offset by 19 mm relative to each other. In configuration "B" the jets were aligned (no offset) relative to each other along both walls of the main channel. The "A-mod" and "B-mod" configurations had the first series of jets blocked. Figure 5 shows the jet spacing and stagger. The red and green lines indicate jet locations and sides.

Initial testing was performed using 25 thermocouples strategically placed in the passage of the channel. A smooth channel with no swirl inducement strategies was tested first, and the results of normalized heat transfer enhancement and pressure losses were used to compare against all tests with jet swirl enhancements. Testing with thermocouples as well as liquid crystal techniques will provide a more detailed account of heat transfer enhancement in the passage.

Heated air enters the test piece via two outer jet supply channels and exits the single flow slot shaped channel. Upon exiting the channel the air is routed through a small plenum, then finally exits through two 18 mm holes to the atmosphere. The main channel inner walls are coated with a specially prepared thermochromic liquid crystal (TLC) substance which turns green at a nominal temperature of 35^0C. Two thin film thermocouples are attached to the walls, one near the entry and one near the exit of the main channel. These will be used to confirm the accuracy of the TLC. Five fine wire thermocouples are placed, equally spaced, in the main channel flow stream. These thermocouples measure the main channel centerline air temperature. The thermocouples are wired directly to a Labview thermocouple data acquisition system. The thermocouples have a resolution of 20 Hz and the data acquisition system is set to read thermocouple data at 15 Hz.

Two Canon SD430 wireless cameras are securely mounted on each side of the test piece. The cameras are set to record video images at 15 Hz. The thermocouple data acquisition system and the video cameras are synchronized via cold cathode fluorescent lamps (CCFL) that are used to illuminate the TLC and are triggered by a switch attached to an air bypass valve.

Prior to the start of a test, heated air is allowed to bypass the test section. Once the bypassed heated air temperature has stabilized at approximately 80^o C preparations for the start of a test begins. The test piece is also maintained at room temperature for an extended period prior to the start of a test to ensure a uniform initial temperature.

As stated, the combined mass flow rate at the exit of the test piece is used to determine an equivalent Reynolds number for comparison with the baseline tests that do not utilize jets or orifices.

To begin a test, the thermocouple data acquisition system is activated and the cameras begin recording. Then a bypass valve is closed allowing heated air to enter the test piece. Video images and thermocouple temperature readings are stored for post test processing. The basic layout of the test apparatus is shown in figure 6.

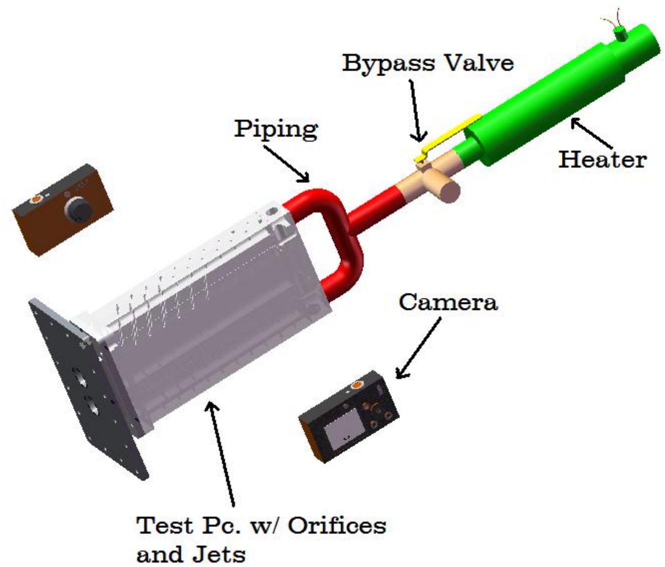

FIGURE 6: BASIC LAYOUT OF TEST APPARATUS

Heat Transfer Coefficients

The local heat transfer coefficients across a liquid crystal coated target surface can be obtained using the 1-D transient heat conduction model of a semi-infinite solid with a convective boundary condition as given by:

$$\frac{\partial^2 T}{\partial x^2} = \frac{1}{\alpha}\frac{\partial T}{\partial t} \tag{1}$$

with boundary and initial conditions:

$$\begin{aligned} &\text{at } t = 0,\ T = T_i \\ &\text{at } x = 0,\ -k\frac{\partial T}{\partial x} = h(T_w - T_m) \\ &\text{at } x \to \infty,\ T = T_i \end{aligned} \tag{2}$$

where, h is the surface heat transfer coefficient, T_w is the time-varying wall surface temperature and T_m is the time-varying local centerline (for internal flows) temperature. This is measured in the present work using suspended centerline thermocouples at several axial locations. These suspended thermocouples acquire temperature changes throughout each test. The data is used to produce a curve fit of the centerline temperatures vs. time along the entire main channel. The temperature vs. time equation is then associated with each column of pixels in the video image. Therefore, each column of pixels (flow stream is along rows) has an associated time vs. temperature array of data.

The solution for the surface temperature response with time is:

$$\frac{T_w - T_i}{T_m - T_i} = 1 - \exp\left(\frac{h^2 \alpha t}{k^2}\right) \operatorname{erfc}\left(\frac{h\sqrt{\alpha t}}{k}\right) \quad (3)$$

A single transient test using the liquid crystal method described earlier is used. Each pixel value is examined for its peak in local intensity. The intensity value is used in conjunction with a specifically written MATLAB program to determine the corresponding temperature. By measuring the corresponding time required for the surface to reach this temperature, the local heat transfer coefficient can be determined.

The 1D semi-infinite solid assumption must be satisfied. In order to satisfy the semi-infinite assumption, the transient temperature must not penetrate through the thickness of the polycarbonate during the test duration. This is achieved by a sufficiently thick test piece of low thermal conductivity and diffusivity (0.201 W/mK and 0.1046 x10^{-6} m^2/s for polycarbonate respectively). For the one-dimensional heat transfer assumption to be satisfied, conduction should only occur normal to the surface with all lateral conduction effects neglected. The test piece may actually experience some lateral conduction, but it is assumed that the dominant temperature gradient is in the direction perpendicular to the surface, and lateral effects are negligible.

Although the initial temperature of the polycarbonate is uniform at ambient temperature, the incoming fluid temperature is higher and not a linear step increase. This is accounted for through the modification of the previous equation by Duhamel's superposition theorem, which represents the temperature change as a series of steps described by:

$$T - T_i = \sum_{i=1}^{N}\left[1 - exp\left(\frac{h^2}{k^2}\,\alpha(t-\tau_i)\right) erfc\left(\frac{h}{k}\sqrt{\alpha(t-\tau_i)}\right)\right] \Delta T_{m,i} \quad (4)$$

where, τ is the time step for each temperature step, $\Delta T_{m,i}$ is the temperature difference between each temperature step and the initial temperature, T_i, α, and k are characteristic of the polycarbonate plate. The temperature of the fluid exiting the jets as expansion occurred is not known, but is assumed to be taken into account when the main channel centerline temperature vs. time data is obtained.

Pressure Tests

A pressure tap is located at each end of the main channel and at each end of the outer jet supply channels. In order to obtain accurate and consistent results, pressure measurements were taken during steady state adiabatic tests. The pressure differential between the inlet of the jet supply channel and the inlet of the main channel was used to determine the percentage of mass flow that entered the main channel, with the mass flow through the orifice calculated using equation 5. The orifices were manufactured to ISO 5167 standard dimensions and the mass flow through the orifice was calculated using the standard equation for compressible non-choked flow through an orifice as shown in equation 5.

$$\dot{m} = C\, A_2\, P_1 \sqrt{\frac{2\,M}{Z\,R\,T_1}\left(\frac{k}{k-1}\right)\left[(P_2/P_1)^{2/k} - (P_2/P_1)^{(k+1)/k}\right]} \quad (5)$$

Flow meters were positioned before the heater which supplied heated air to each jet supply channel. The measured mass flow rate and pressure, temperature, and cross section area at the entry of each channel was used to determine velocities, densities, and associated Reynolds numbers, where applicable.

Pressure drops along the main channel and outer channels are recorded and used to determine pressure losses. Normally, friction losses are calculated and used to determine overall thermal performance. The generally accepted method for calculating the overall thermal performance (OTP) is shown in equation 6,

$$OTP = \frac{N_u/N_{uo}}{\left(f/f_o\right)^{1/3}} \quad (6)$$

where, Nu/Nu_o is the heat transfer enhancement, f is the overall friction loss in the test piece, and f_o is the overall friction loss in a smooth pipe of the same hydraulic diameter.

The relationship between friction loss and pressure loss is shown in equation 7.

$$f = 2\, d_h \frac{\Delta P}{L\,\rho\,U^2} \quad (7)$$

The complexity of the flow passages, along with the multiple length scales (jet hole diameter, main channel hydraulic diameter, side channel diameter) and associated velocity scales preclude an easy adaptation of equation (7) above to calculate friction factor. Instead, the equation for OTP was modified to use an overall pressure drop ratio instead of a friction factor ratio. For these tests, equation 8 was used to calculate the overall thermal performance (OTP).

$$OTP = \frac{\frac{Nu}{Nu_{90\,smooth}}}{\left(\frac{\Delta P}{\Delta P_{90\,smooth}}\right)^{1/3}} \qquad (8)$$

In this equation the $Nu_{90\ smooth}$ value is the Nusselt number associated with flow through the test piece without the orifices installed and flow through all jets blocked. The value $\Delta P_{90\ smooth}$ is the pressure loss in the same plain test piece. The pressure tap locations are shown in figure 7. When the orifices are introduced into the system the total pressure drop of the system is considered. In figure 7, this would be the pressure drop from $P_{1\ outer}$ (pressure before the orifices) to $P_{2\ main}$ (pressure near the exit of the channel). All heat transfer enhancement values reported were normalized to the same standard slot shaped channel with a 90 degree entry.

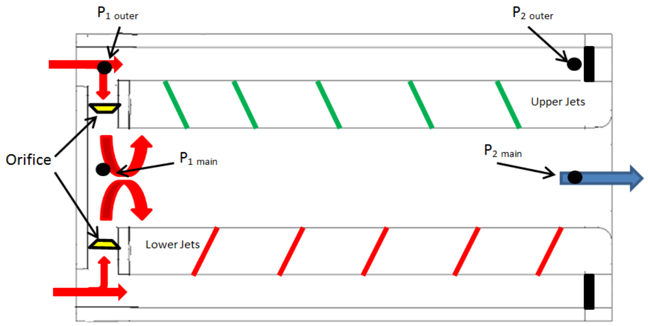

$\Delta P = P_{1\ outer} - P_{2\ main}$

FIGURE 7: PRESSURE TAP LOCATIONS USED FOR PRESSURE LOSS CALCULATIONS.

EXPERIMENTAL UNCERTAINTY AND ERROR

An accurate assessment of uncertainty in liquid crystal measurement of heat transfer coefficients is essential because many factors affect the TLC results. A large number of studies have concluded that a properly performed test yields mean uncertainly of up to 11.0% for values of h, and up to 9% for temperatures. Smith [9], et al, compiled a table summarizing uncertainty studies of h and T when narrow band TLC methods were used. Thermocouple accuracy and repeatability are large contributors to uncertainty as well as illumination spectral effects. The wall mounted thermocouples were used to compensate for this effect and resulted in a 0.2^o C temperature correction.

A minimum of two of each test was conducted to evaluate repeatability. Heat transfer values typically were repeatable within 3% -5% for tests with Reynolds numbers up to 25,000 and repeatability of 5%-8% with Reynolds number tests up to 50,000. As reported in the literature [9], current estimates of the uncertainty in the Nusselt number are approximately 10%.

RESULTS AND DISCUSSION

It is hypothesized that the angle and location of the jets and orifices provide several positive heat transfer effects. The high velocity air issuing from the jets placed tangent to the walls of the main channel creates a high-shear flow phenomenon as the air travels along the walls of the main channel. High-shear can potentially lead to high heat transfer regions. As the air passes through the orifices, which oppose each other near the entry of the main channel, the velocity increases, and the high velocity air from each end collides and creates high turbulence at the 90 degree channel entry. The high turbulence at entry can potentially lead to high heat transfer coefficients.

The position of the jets in configuration “A” and “A-mod” is such that the high velocity side-jet flow continues across the main channel, and proceeds around the end walls of the slot shaped channel. This jet flow encounters the high velocity jet stream exiting the succeeding jet on the opposite wall. It is hypothesized that the angle and location of the jets and orifices provide several positive heat transfer effects. Additionally, when the lower velocity main channel air engages the high velocity jets in cross flow, the low velocity main channel air tumbles over the high velocity jets which act as pseudo-helical trip strips. The turbulence intensity grows as the main channel air proceeds along the flow path. Figure 8 shows this postulated phenomenon as increasing spirals attached to the imaginary helical strips created by the high velocity jets.

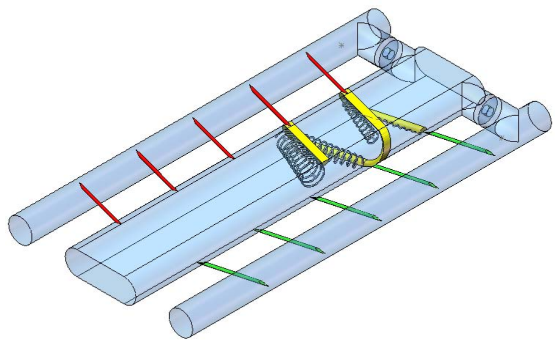

FIGURE 8: CONCEPT OF SWIRL AND TUMBLE CREATED BY ANGLED JETS ON EACH SIDE OF SLOT SHAPED CHANNEL.

Jet configurations “B” and “B-mod” offer a different swirl and tumble phenomenon, as the opposing jets are not offset.

In order for these configurations to work in a practical environment there must exists a pressure differential between the flow exiting the turbine airfoil, usually through film cooling holes, and the local pressure outside of the airfoil. A safety margin must be established to prevent high temperature combustion gases from entering the interior of the airfoil. The concept of Back Flow Margin (BFM) is shown in Equation 9. The value of margin varies per location.

$$\%BFM = \frac{P_{int} - P_{ext}}{P_{ext}} * 100\% \quad (9)$$

The pressure loss ratio values for each configuration and associated orifice diameter are shown in table 1. The ΔP values are the pressure losses that occur from the outer jet supply channel inlet (the high pressure side of the orifice) minus the main channel exit pressure.

Smooth Channel w/ 90 deg. Inlet (3.18mm Orifice)		
Reynolds Number (10^3)	$\Delta P_{A\ or\ B} / \Delta P_{smooth}$	$\Delta P_{A\text{-}mod\ or\ B\text{-}mod} / \Delta P_{smooth}$
10	52.8	67.6
25	54.1	70.0
40	49.2	66.5
50	45.1	59.7

Smooth Channel w/ 90 deg. Inlet (3.94mm Orifice)		
Reynolds Number (10^3)	$\Delta P_{A\ or\ B} / \Delta P_{smooth}$	$\Delta P_{A\text{-}mod\ or\ B\text{-}mod} / \Delta P_{smooth}$
10	39.9	44.0
25	39.3	37.9
40	38.1	35.9
50	43.9	41.6

Smooth Channel w/ 90 deg. Inlet (4.76mm Orifice)		
Reynolds Number (10^3)	$\Delta P_{A\ or\ B} / \Delta P_{smooth}$	$\Delta P_{A\text{-}mod\ or\ B\text{-}mod} / \Delta P_{smooth}$
10	19.6	22.0
25	20.3	25.1
40	21.2	25.9
50	18.6	23.3

TABLE 1: RATIO OF PRESSURE LOSS ($\Delta P/\Delta P_{smooth}$) FOR EACH CONFIGURATION AND ORIFICE DIAMETER.

Because of the equal number of jets in configuration “A” and “B”, and in “A-mod” and “B-mod” the pressure loss values are the same for the associated orifice diameter.

The pressure loss values are within reason for preventing back flow in many turbine engines for which published data is available. The orifice diameter is the major contributor to the pressure loss. This feature of the cooling strategy can be tailored to a specific application to ensure that a safe BFM is maintained.

There exists substantial heat transfer benefits with the opposing passages and 90 degree turn at the inlet of the slot shaped channel when compared to a smooth round pipe of equal hydraulic diameter. Figure 9 shows the normalized Nusselt number (Nu/Nu_o) plots for the slot shaped channel with three different entry setups, all with an equivalent Reynolds number of 10,000. The first one labeled “case 1” is a color contour plot of the slot shaped channel with an axial flow entry path. In this case, the flow traveled radially through a rectangular channel with dimensions approximately 1.5 times that of the slot channel. The flow transitioned from the square channel into the slot shaped channel via a 12.5 mm radiused entry. The normalized channel averaged Nusselt number is 1.04. The pressure loss is very low. This configuration yields an OTP of 1.01 and essentially duplicated results similar to fully developed flow in a smooth round pipe.

The second plot labeled “case 2” is the slot shaped channel with a 90 degree entry, all side-jets blocked, and no orifices installed in the opposing entry channels. The entry channels are 15.9 mm diameter round passages. The velocity at the inlet is much higher than in case “1”, but still much lower when compared to the entry velocity with orifices installed.

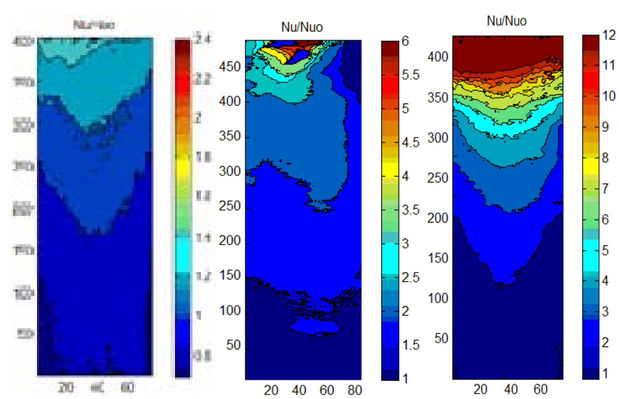

case 1 **case 2** **case 3**

FIGURE 9: Nu/Nu_o COLOR CONTOUR PLOTS FOR Re_{eq} = 10k FOR; case 1) AXIAL INLET w/ RADIUSED ENTRY, case 2) 90 DEGREE INLET w/o ORIFICES AND BLOCKED JETS, case 3) 90 DEGREE INLET WITH 3.18 mm ORIFICES AND BLOCKED JETS.

As indicated in the plot, the effect of the fluid interaction of the opposing passages leads to Nu/Nu_o values near 6 at the inlet. The normalized channel averaged Nusselt number is 1.93 and the overall thermal performance is 0.87.

In “case 3”, two 3.18 mm orifices were installed in the opposing entry channels. As expected, the heat transfer enhancement is very high near the inlet of the channel due to the high velocity colliding air streams that direct air into the main slot shaped channel. The high velocity coupled with higher turbulence levels expected due to jet-impingement results in local Nu/Nu_o values of 12 near the entry of the channel. The high turbulence reduces as the flow progresses through the channel and the Nu/Nu_o values are near 1.0 at the exit of the channel. The normalized Nusselt number for this configuration is 4.85. The pressure losses are very high in this case due to the orifices and the OTP is a mere 0.29. The high heat transfer performance at the entry of the channel was the primary cause for testing in the A-mod and B-mod configurations. The hypothesis was that the orifices would create enough turbulence near the channel entry that jets would not be needed.

With the orifices and jets installed, calculations determined the distribution of mass flow through the jets and through the orifices. The mass flow rate associated with each Reynolds number and percent mass flow through the jets for the various orifice diameters and jet configurations are shown in table 2. The mass flow through the entry of the main channel varied from about 20 % - 40%, depending on the test configuration and Reynolds number.

		% Mass Flow Through All Jets					
Reynolds Number	Total Mass Flow Rate (kg/s)	3.18 mm Orifice (A, B)	3.94 mm Orifice (A, B)	4.76 mm Orifice (A, B)	3.18 mm Orifice (Amod, Bmod)	3.94 mm Orifice (Amod, Bmod)	4.76 mm Orifice (Amod, Bmod)
10,000	*0.00543*	73.1%	62.9%	61.3%	70.2%	60.3%	58.0%
25,000	*0.01353*	77.6%	70.1%	68.2%	73.2%	67.3%	64.3%
40,000	*0.02165*	79.0%	73.0%	70.4%	76.1%	72.3%	67.5%
50,000	*0.02706*	79.3%	75.7%	72.5%	78.4%	74.6%	69.2%

TABLE 2: PERCENT MASS FLOW RATES THROUGH JETS

The average jet velocities were determined by using the average of the outer channel entrance and end pressures as well as the main channel entry and exit pressures. The difference in jet velocity from the first jet to the last jet is not shown in detail, but is calculated to be as small as 3 m/s in the case of the 4.76 mm orifice in conjunction with a Re=10k, to a difference of 21 m/s in the case of the 3.18 mm orifice in conjunction with a Re=50k. The blowing ratio (BR), which is defined as the ratio of the average jet velocity to the average main channel velocity, and the average jet velocity are shown in table 3. Since the temperature of the heated air averaged approximately 60^o C and the Mach number of air is related primarily to temperature (and humidity), the corrected choke velocity is ~367 m/s. Under the worst case conditions the flow through the orifices never exceeded M = 0.4, and thus the compressible flow equation is valid for measuring flow and accurately determining effective mass flow and equivalent Reynolds number.

	Average Jet Velocity, m/s and (Blowing Ratio)					
Reynolds Number	3.18 mm Orifice (A, B)	3.94 mm Orifice (A, B)	4.76 mm Orifice (A, B)	3.18 mm Orifice (Amod, Bmod)	3.94 mm Orifice (Amod, Bmod)	4.76 mm Orifice (Amod, Bmod)
10,000	73 (36)	55 (10)	42 (9)	92 (40)	66 (16)	50 (15)
25,000	183 (36)	114 (12)	73 (10)	201 (44)	114 (16)	87 (15)
40,000	221 (36)	182 (17)	116 (14)	268 (44)	211 (19)	129 (15)
50,000	269 (40)	222 (19)	131 (14)	291 (41)	243 (20)	154 (16)

TABLE 3: AVERAGE JET VELOCITY AND BLOWING RATIO

Nu/Nu_o plots are provided for several of the configurations tested. The channel averaged $Nu/Nu_{90\ smooth}$ and overall thermal performance (see equation 8) values are indicated for each plot. In all these plots, the main flow direction is oriented from the bottom of the figure toward the top.

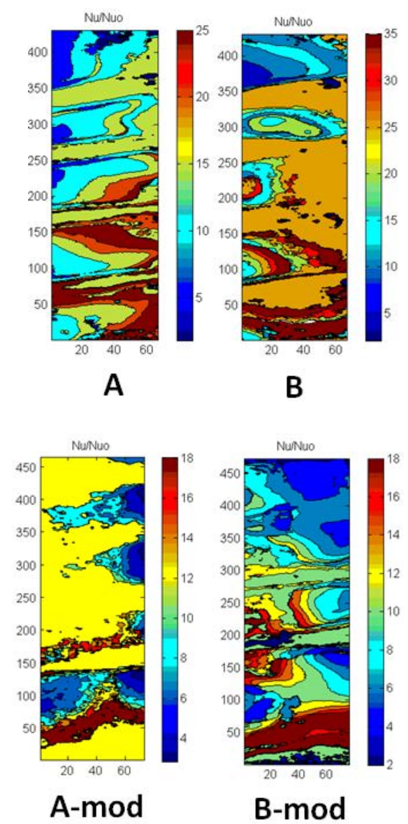

FIGURE 10: Nu/Nu_o PLOTS, 3.18mm ORIFICES, Re_{eq} = 25k

The Re = 10k tests did not yield high OTP values. This is likely due to the low jet velocities. As the jet velocities became higher, accompanied with higher blowing ratios, the OTP values improved. Figure 10 shows color plots of Nu/Nu_o for tests performed with 3.18 mm orifices and mass flow rates equivalent to that of a Re=25k tests with the plain channel.

The $Nu/Nu_{90\ smooth}$ values were 9.62, 10.68, 8.18, and 7.26, and OTP values were 2.55, 2.83, 1.99, and 1.76 for the A, B, A-mod, and B-mod configurations, respectively. The B and A-mod configurations showed very good uniformity in the heat transfer distribution. The jet signatures were not as sharply defined as in some tests with higher jet velocities. This proved to be a beneficial in creating a more uniform heat transfer channel.

When the largest orifices were used the blowing ratio was less than half of those with the smallest orifices and the jet velocities were significantly reduced. The $Nu/Nu_{90\ smooth}$ values for the largest, 4.76 mm orifices tested at Re=25k were 6.15, 3.30, 5.49, and 3.70 and the OTP values were 2.25, 1.21, 1.87, and 1.26 for the A, B, A-mod, and B-mod configurations, respectively.

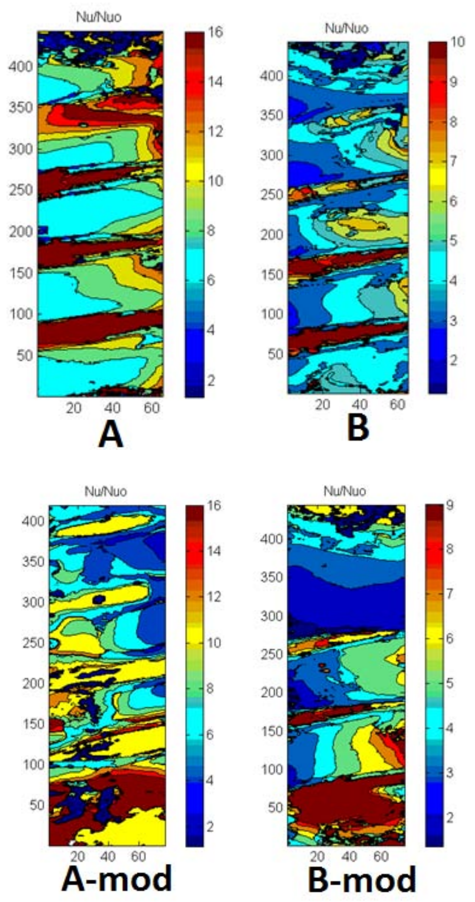

FIGURE 11: Nu/Nu_o PLOTS, 4.76mm ORIFICES, Re_{eq} = 25k

Figure 11 shows the color contour plots for this scenario. In this case configuration A has the best OTP and reasonable good distribution throughout the entire main channel. These values are considerably lower than those in the figure 10.

The data obtained and color plots in figure 12 shows the values of $Nu/Nu_{90\ smooth}$ were 6.44, 5.10, 5.72, and 7.60, and OTP values were 1.92, 1.52, 1.73, and 2.30 for the A, B, A-mod, and B-mod configurations, respectively.

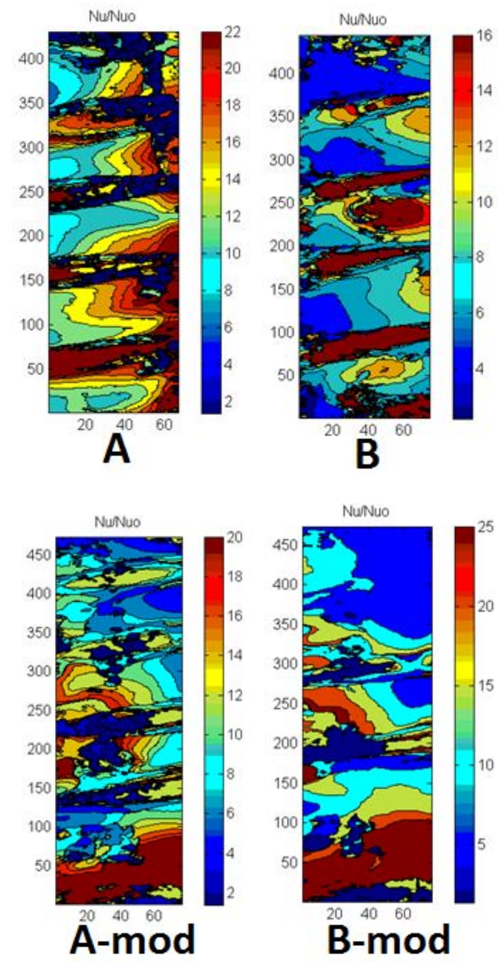

FIGURE 12: Nu/Nu_o PLOTS, 3.94mm ORIFICES, Re_{eq} = 40k

The high heat transfer zones near on one end of the channel contributed to the high OTP of the B-mod configuration. The distribution was better for the A configuration.

At the highest Reynolds number tested and the largest orifices, the blowing ratios ranged from 10 to 19 and the jet velocities ranged from 131 m/s for configurations A and B, and 154 m/s for configurations A-mod and B-mod. The values of $Nu/Nu_{90\ smooth}$ were 4.19, 5.75, 5.43, and 5.24, and OTP values were 1.58, 2.17, 1.90, and 1.83 for the A, B, A-mod, and B-mod configurations, respectively. The color contour plots in figure 13 show that configuration B provides good reasonably even distribution throughout the channel.

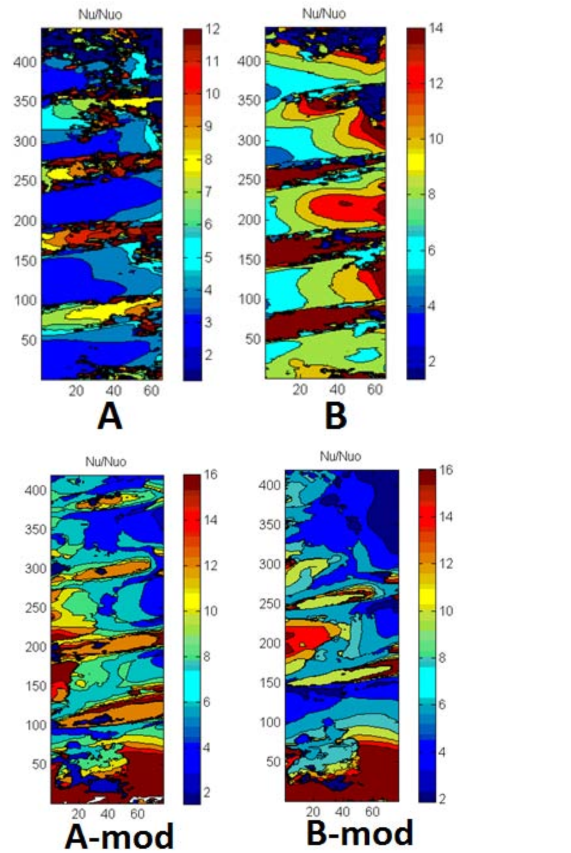

FIGURE 13*: Nu/Nu$_o$ PLOTS, 4.76mm ORIFICES, Re$_{eq}$ = 50k*

A summary of the Nu/Nu$_{90\ smooth}$ values are presented in the data points of figures 14 and 15. The data clearly shows the superior performance of several combinations of orifice and jets at the equivalent Reynolds number of 25,000.

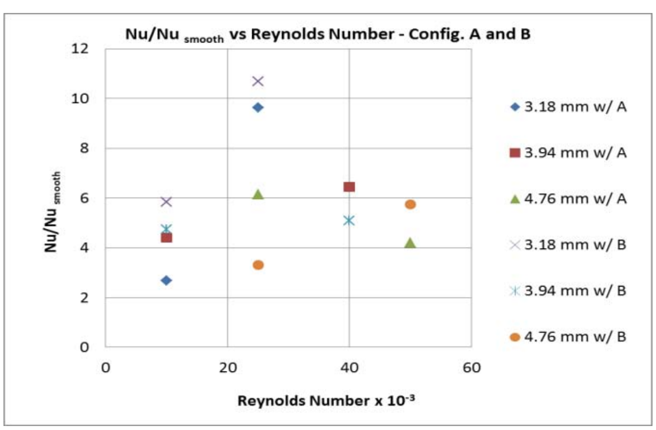

FIGURE 14: Nu/Nu $_{90\ smooth}$ vs. REYNOLDS NUMBER FOR ALL ORIFICES, CONFIGURATIONS A and B.

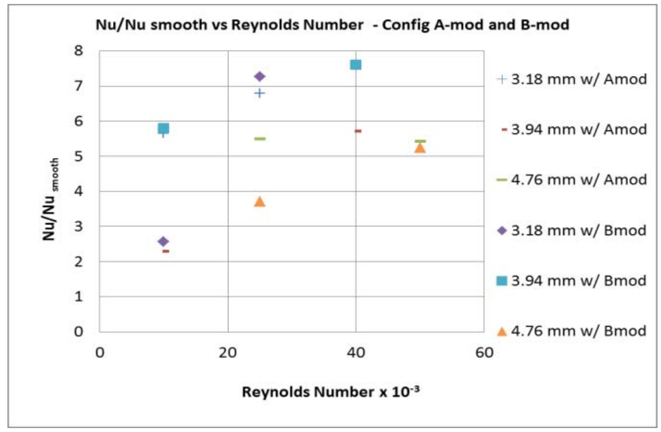

FIGURE 15: Nu/Nu $_{90\ smooth}$ vs. REYNOLDS NUMBER FOR ALL ORIFICES, CONFIGURATIONS A-mod AND B-mod.

This is not surprising, as the d/b and p/d values used were chosen based on testing performed with trip strips that performed well at Reynolds numbers near 25k, using similar ratios [2,3,4].

If the values in figures 14 and 15 were viewed without considering the pressure losses, most tests configurations would appear superior to trip strips and other mid-span heat transfer enhancement techniques. But the pressures losses incurred in each of these tests were substantial, as shown in Table 1. Equation 8 was used to calculate the overall thermal performance. The result of merging the data in figures 14 and 15 with the pressure loss ratios in table 1 are displayed as overall thermal performance values (OTP) in figures 16 and 17. All of the 10,000 Reynolds number tests were low performers, while most of the higher Reynolds number test yielded OTP values above 1.5. The low velocity jets and orifices of the Re=10k tests showed reasonable good heat transfer distribution, but did not perform well when pressure losses were included.

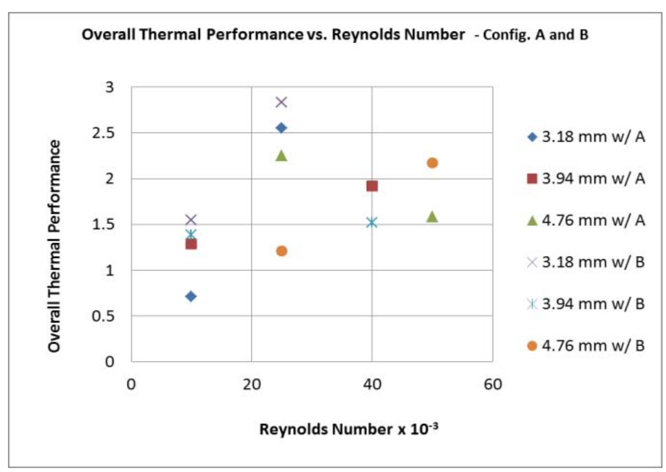

FIGURE 16: OTP vs. REYNOLDS NUMBER FOR ALL ORIFICES, CONFIGURATIONS A and B.

The Re = 25,000 tests performed the best with the 3.18mm orifices in jet configurations A and B. The Re=40k and Re=50k tests with jets in configurations A and B performed best with the larger diameter orifices.

With the jets configured in the A-mod and B-mod setups the majority of the tests produced reasonable good performance throughout the range of Reynolds numbers. The standout performer was the 3.94 mm orifices with jets setup in the B-mod layout at Re = 40k.

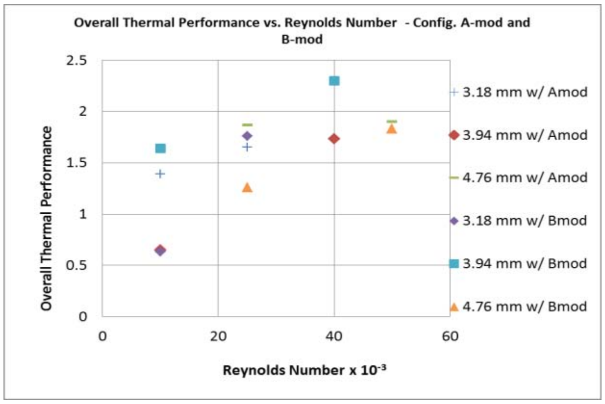

FIGURE 17: OTP vs. REYNOLDS NUMBER FOR ALL ORIFICES, CONFIGURATIONS A-mod AND B-mod.

CONCLUSIONS

The heat transfer properties of a new and unique multi-channel passage, consisting of a 3:1 aspect ratio slot shape channel with jets issuing from each side and circular outer channels that connected the outer channels to the main channel, was tested for a range of mass flow rates and associated equivalent Reynolds numbers of 10,000 to 50,000. The high velocity side jets entered the main channel flow at a 15 degree angle relative to the main flow direction at average blowing ratios ranging from 9 to 40. As the main channel flow entered the channel from a 90 degree inlet, through an orifice, the flow encountered high velocity jets issuing along the walls of the slot channel. The orifices were a major contributor to high pressure losses through the test piece. The pressure losses were taken into account in the heat transfer performance values (OTP). In addition to the jets having a shearing/impingement type affect along the floor at the exit of the jet, the jets ideally acted as pseudo-trip strips for the main channel fluid contacting the jets stream in cross flow.

Overall Thermal Performance (OTP) values as high as 2.83 are reported and many of the various configuration show good heat transfer distribution throughout the main channel. This concept offers a new alternative for turbine airfoil designers as long as an acceptable back flow margin (BFM) can be maintained.

ACKNOWLEDGEMENTS

The authors wish to thank the Clean Power and Energy Research Consortium for funding this project. We also would like to acknowledge Brunet Breaux for his assistance in conducting many of the tests, Dr. Yi Liang for his assistance with the Matlab computer programming used to analyze the test results, and Norbert Sigue for fabricating many of the components used in the tests.

REFERENCES

[1] Wagner, J. H., Johnson, B. V., Graziani, R. A. and Yeh, F. C., 1992. "Heat Transfer in Rotating Serpentine Passages With Trips Normal to the Flow". *J. Turbomachinery, Trans. ASME*, **114**, pp. 847-857.

[2] G. Tanda, 2004. “Heat transfer in rectangular channels with transverse and V-shaped broken ribs”. *International Journal of Heat and Mass Transfer*, .**47**, pp. 229–243.

[3] Lei Wang, Bengt Sunden, 2007. “Experimental Investigation of Local Heat Transfer in a Square Duct with Various-shaped Ribs”. *Heat Mass Transfer*, **43**, pp. 759-766.

[4] Taslim, M.E., Li, T., Kercher, D.M., 1996. “Experimental Heat Transfer and Friction in Channels Roughened With Angled, V-Shaped, and Discrete Ribs on Two Opposite walls”. *Trans. ASME, Journal of Turbomachinery*, **118**, pp. 20-28.

[5] İrfan Kurtbaş, 2009. “Heat transfer augmentation by swirl generators inserted into a tube with constant heat flux”. *International Communications in Heat and Mass Transfer*, **36**, pp. 865–871.

[6] Hedlund, C. R., Ligrani, P. M., Moon, H. K., and Glezer, B., 1998. “Heat Transfer and Flow Phenomena in a Swirl Chamber Simulating Turbine Airfoil Internal Cooling”. ASME Paper 98-GT-466.

[7] Glezer, B., Moon, H. K., Kerrebrock, J., Bons, J., and Guenette, G., 1998. “Heat Transfer in a Rotating Radial Channel with Swirling Internal Flow,” ASME Paper 98-GT-214.

[8] Bunker, R.S., 2004. “Latticework (Vortex) Cooling Effectiveness Part 1: Stationary Channel Experiments”. ASME Paper No. GT-2004-54157.

[9] C.R. Smith, D.R. Sabatino, and T.J. Praisner, 2001. “Temperature sensing with thermochromic liquid crystal”. *Experiments in Fluids*, **30**, pp. 190-201.